

The Unusual Weak-Line Quasar PG1407+265 and its Foreground $z \sim 0.7$ X-ray Cluster

JONATHAN C. McDOWELL,¹ ANETA SIEMIGINOWSKA,¹ MATTHEW ASHBY,¹ KATHERINE BLUNDELL,² AND LUIGI C. GALLO³

¹*Center For Astrophysics — Harvard & Smithsonian
60 Garden St,
Cambridge, MA 02138, USA*

²*Department of Physics, University of Oxford, Keble Rd, Oxford OX1 3RH, UK*

³*Department of Astronomy & Physics, Saint Mary's University, 923 Robie Street, Halifax, Nova Scotia, B3H 3C3, Canada*

(Accepted 2021 Jun 9)

Submitted to ApJ

ABSTRACT

We present new observations of the odd $z = 0.96$ weak-line quasar PG1407+265, and report the discovery of CXOU J140927.9+261813, a $z = 0.68$ X-ray cluster. Archival X-ray photometry spanning nearly four decades reveals that PG1407+265 is variable at the 1 dex level on a timescale of years. V-band variability is present with an amplitude less than 0.1 mag. The emission-line properties of PG1407+265 also reveal clear evidence for a powerful inflow or outflow due to near- or super-Eddington accretion, having a mechanical luminosity of order $10^{48} \text{ erg s}^{-1}$. Our follow-up *Chandra* exposure centered on this object reveal a foreground $z = 0.68$ cluster roughly $1' \times 1'.5$ in extent, offset to the east of PG1407+265, roughly coincident with the $z = 0.68$ radio galaxy FIRST J140927.8+261818. This non-cool-core cluster contributes about 10% of the X-ray flux of PG1407+265, has a mass of $(0.6 - 5.5) \times 10^{14} M_{\odot}$, and an X-ray gas temperature of $(2.2 - 4.3) \text{ keV}$. Because the projected position of the quasar lies at about twice that of the cluster's inferred Einstein radius, lensing by the cluster is unlikely to explain the quasar's unusual properties. We also discuss the evidence for a second cluster centered on and at the redshift of the quasar.

Keywords: quasars

1. INTRODUCTION

The prototypical X-ray-loud weak-line quasar (WLQ), PG 1407+265, is a luminous $z \sim 1$ AGN with a probable strong outflow (see Section 2) but only a weak, albeit relativistic, radio jet on parsec scales (Blundell et al. 2003). This distinguishes it from the X-ray weak WLQs studied by Luo et al. (2015) and the reason for its unusual properties - such as weak emission lines and large line velocity shifts McDowell et al. (1995) - remains unresolved.

Luminous AGN are frequently found in BCGs (Brightest Cluster Galaxies) - the massive elliptical galaxies in the centers of clusters. Such luminous quasars, hosting supermassive black holes (SMBH) with masses $> 10^9 M_{\odot}$ (McConnell et al. 2011, McConnell et al. 2012), are believed to be growing via accretion at near-Eddington rates. Optical studies by Ellingson et al. (1991) showed that radio-loud quasars in particular are often found in rich clusters. Cluster formation at $z > 1$ must have been influenced by the quasar phase of the BCG, and so studies of the properties of clusters hosting such quasars provide important information about the connection between the BCG and the cluster halo, the cluster heating and the feedback process, as well as cluster scaling relations and evolution. However, there are few known X-ray-luminous clusters associated with bright quasars at redshifts low enough for detailed study - e.g. 3C186 at $z = 1.2$ (Siemiginowska et al. 2005, Siemiginowska et al. 2010), H1821+643 at $z = 0.30$ (Russell et al. 2010), PKS1229-021 at $z = 1.05$ (Russell et al. 2012). Detecting such clusters in the presence of the bright quasar

X-ray emission has proven challenging. Surveys using the high spatial resolution of *Chandra* are only now revealing previously missed clusters (e.g. CHiPS, Somboonpanyakul et al. 2021).

Here we report the detection of diffuse X-ray emission in the XMM image of PG1407+265, together with followup high spatial resolution X-ray observations with *Chandra* and optical spectroscopy of galaxies in the field. We report the discovery of a foreground ($z = 0.68$) X-ray cluster along the line of sight, and describe what is now known about the unusual quasar PG1407+265.

In this paper we adopt the Planck 2018 cosmology of $H_0 = 67.4 \text{ km s}^{-1} \text{ Mpc}^{-1}$, $\Omega_\Lambda = 0.685$ (Planck Collaboration et al. 2020).

2. PG1407+265: AN EXTREME, FACE-ON, OUTFLOWING AGN

Discovered in the Palomar Green survey (Schmidt & Green 1983) as a 15th-magnitude object, an extensive multiwavelength study (McDowell et al. 1995) confirmed PG1407+265’s classification as a quasar and drew attention to its unusual combination of emission lines with very low equivalent widths and large velocity shifts. Specifically, the high-ionization lines are blueshifted up to 13000 km s^{-1} relative to the low-ionization ones, and could indicate a massive outflow (see e.g. Tadhunter 2008). This X-ray-bright and optically bright AGN has been observed by *Einstein*, *Rosat*, *Ginga*, *ASCA* and *XMM* (Fig. 1, Table 1), but never previously by *Chandra*. Comparison of the historical X-ray observations from 1981 to 2001 shown in Figure 1 and detailed in Table 1 indicates that the quasar varies by an order of magnitude in X-ray luminosity, well in excess of the uncertainties of cross-mission comparison. The XMM data (Gallo 2006) revealed factor of 2 variability on several-month timescales, with high and low spectral states interpreted as being due to the known jet variability on parsec scales (Blundell et al. 2003).

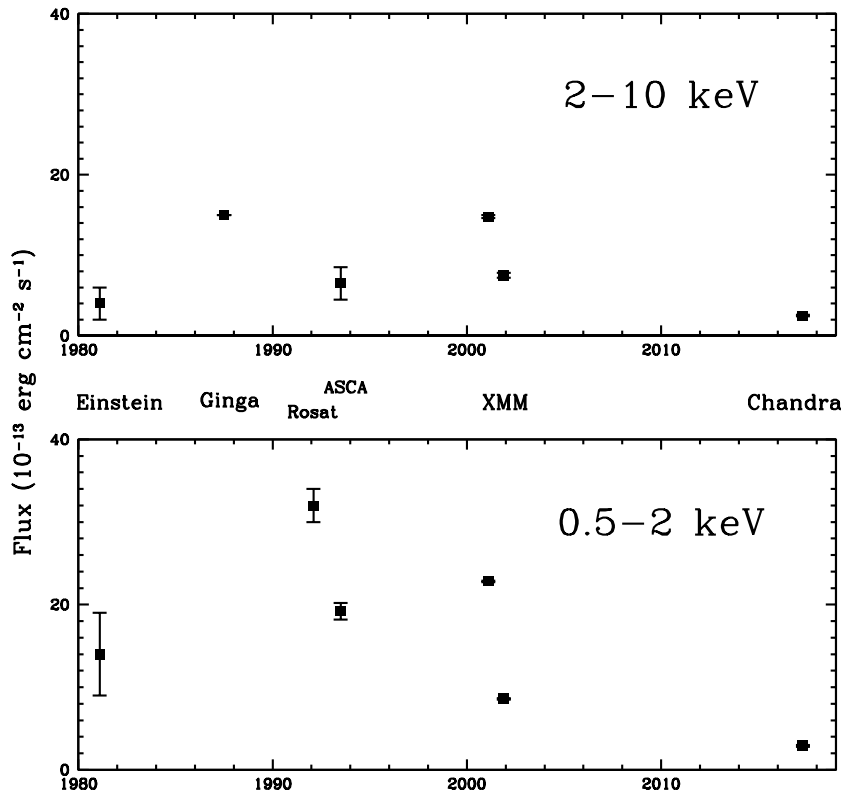


Figure 1. Historical X-ray light curve of PG1407+265. Upper panel: Flux in 2-10 keV energy range. Lower panel: Flux in 0.5-2 keV energy range. See Table 1 for observational details and references.

Optical spectrophotometry (McDowell et al. 1995) showed that the low-ionization lines such as $\text{H}\alpha$ have a redshift $z = 0.96$, while the high-ionization lines such as CIV have a significantly lower redshift of $z = 0.92$, indicating the presence of a fast outflow or inflow. We tentatively take $z = 0.96$ to represent the system redshift, since the low-ionization lines are unlikely to be part of the outflow. Absorption features at $z=0.575$, 0.600 , 0.683 , and 0.817 have

Date	Instrument	Seq	Absorbed Flux 0.5-2 keV	($10^{-13} \text{ erg cm}^{-2} \text{ s}^{-1}$) 2-10 keV	Ref
1981 Jan	Einstein IPC	5381	14 ± 5	4?	Elvis et al. (1994)
1987 Jun	Ginga LAC		-	15	Williams et al. (1992)
1992 Jan	Rosat PSPC-B	RP700359	32 ± 2	-	McDowell et al. (1995)
1993 Jul	ASCA	70024000	19 ± 1	7 ± 1	Reeves & Turner (2000)
2001 Jan	XMM EPIC	0092850101	22.8 ± 0.1	14.8 ± 0.2	Gallo (2006)
2001 Dec	XMM EPIC	0092850501	8.6 ± 0.1	7.5 ± 0.3	Gallo (2006)
2017 Mar	Chandra ACIS	18265	2.9 ± 0.1	2.4 ± 0.1	This paper

Table 1. X-ray observations of PG1407+265 over 36 years. The *Chandra* flux is the lowest level ever observed for this object. Fitted spectral models in the cited papers are used to recalculate fluxes in the 0.5-2 and 2-10 keV bands when these were not given explicitly. Flux uncertainties are approximate and take into account spectral slope uncertainties.

been detected by [Lehner et al. \(2018\)](#) using HST COS, and are presumably absorption due to galaxies along the line of sight.

The Catalina Sky Survey ([Drake et al. 2009](#)) observed PG1407+265 from 2005 to 2013. The observed (Johnson, Vega-based) *V* magnitudes are consistent with the measured $V = 15.7$ from [Schmidt & Green \(1983\)](#) but indicate a 0.07 mag variability on a 2-year timescale (Fig. 2).

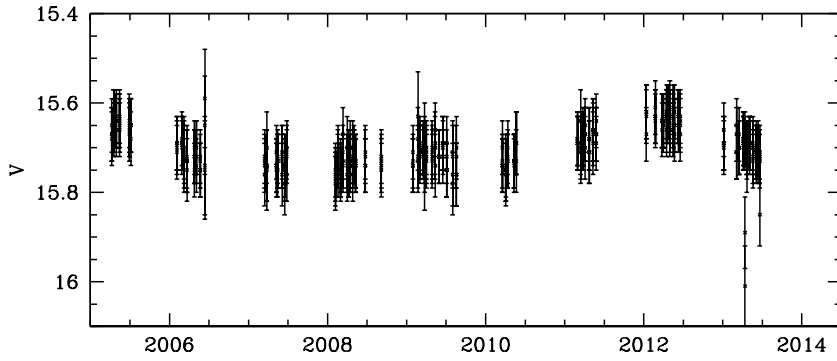


Figure 2. Catalina Sky Survey *V* magnitudes for PG1407+265.

The WISE mid-IR colors of the quasar ([Cutri et al. 2013](#)) are $[3.4]-[4.6] = 1.38$ mag, $[4.6]-[12] = 2.00$ mag. (The WISE photometry bands are identified by $[\lambda]$ where λ is the effective wavelength in microns.) Although the object has some blazar-like properties, it lies at the edge of the locus for normal quasars discussed in [Massaro et al. \(2011\)](#) (Fig. 3).

An updated spectral energy distribution for the quasar is presented in Figure 4. The optical-to-X-ray spectral index is defined as ([Tananbaum et al. 1979](#))

$$\alpha_{ox} = \frac{\log(L(\nu 1)/L(\nu 2))}{\log(\nu 1/\nu 2)}$$

where $\log \nu 1 = 17.684$ corresponding to 2 keV, $\log \nu 2 = 15.079$ corresponding to 2500Å and $L(\nu)$ is the luminosity per unit frequency in the quasar frame. For PG1407+265 the value of α_{ox} prior to the Chandra observations discussed here was -1.26, corresponding to a luminosity-dependent X-ray brightness $\Delta\alpha_{ox}$ relative to typical SDSS quasars ([Gibson et al. 2008](#)) of +0.63, justifying our description of it as ‘X-ray-loud’ compared to the X-ray-normal WLQs found in [Luo et al. \(2015\)](#). However, the fainter state seen in 2017 corresponds to $\alpha_{ox} = -1.68$ or $\Delta\alpha_{ox} = +0.21$, putting the object back in the X-ray-normal range for the time being.

The observed bolometric luminosity of the quasar based on the [McDowell et al. \(1995\)](#) observations was $3.3 \times 10^{47} \text{ erg s}^{-1} = 5.9 M_{\odot} c^2 \text{ yr}^{-1}$ implying a black hole mass of $M = 2.5 \times 10^9 M_{\odot} (L/L_{\text{Edd}})^{-1}$. Using the MgII and

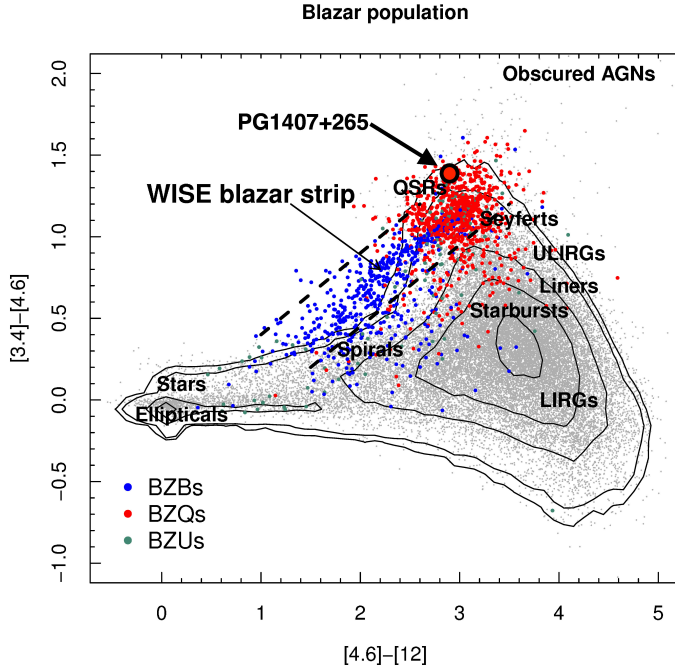


Figure 3. The $[3.4] - [4.6] - [12] \mu\text{m}$ WISE color-color diagram for thermal sources and blazars from Fig. 1 of [Massaro et al. \(2011\)](#), amended to indicate where PG1407+265 lies compared to these populations (large red circle bordered in black). Units are magnitudes. PG1407+265 has $[3.4] - [4.6] = 1.38$ mag, and $[4.6] - [12] = 2.9$ mag. Its mid-infrared colors are similar to those of quasars and to those of the type BZQ blazars defined by [Massaro et al. \(2009\)](#) (i.e. flat spectrum radio quasars with broad emission lines and blazar characteristics, as opposed to classical BL Lacs).

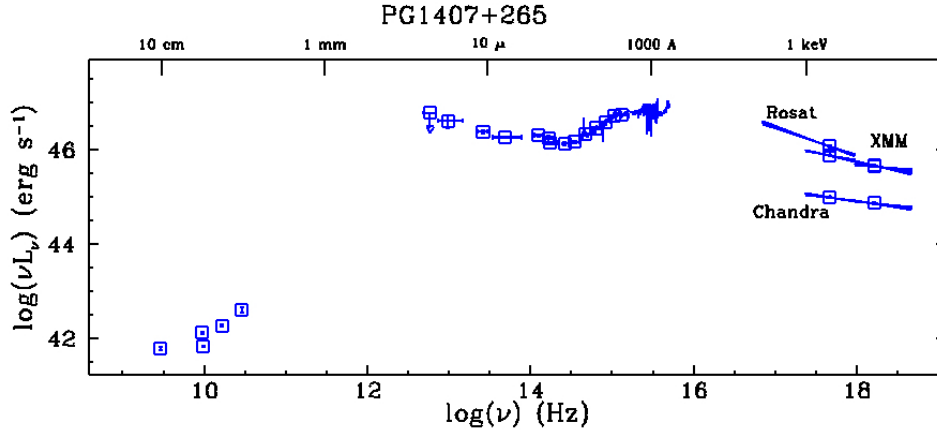


Figure 4. Updated spectral energy distribution of the quasar PG1407+265, dereddened by 0.03 mag and transformed to the rest frame using the Planck cosmology. Compare with Fig 8. of [Elvis et al. 1994](#) which was based on IRAS, IUE and Einstein data. Data from HST are included ([McDowell et al. \(1995\)](#)), as well as from WISE, XMM and Chandra (this paper). Updated VLA data ([Barvainis et al. 1996](#)) and a IRAS 60 micron measurement ([Serjeant & Hatziminaoglou 2009](#)) have been added.

$\text{H}\alpha$ FWHMs and the line width-continuum luminosity mass scaling relationship of [Vestergaard & Osmer \(2009\)](#) we derive a formal black hole mass estimate for PG1407+265 of $1 \times 10^{10} M_{\odot}$ corresponding to $L/L_{\text{Edd}} = 0.25$. However extrapolating the calibration of the relationship to the highest luminosities is uncertain ([Shen & Liu 2012](#)). [Marculewicz & Nikolajuk \(2020\)](#), using an accretion model, estimate a larger mass of $7.9^{+5.1}_{-2.9} \times 10^9 M_{\odot}$ and the true mass is probably at least $5 \times 10^9 M_{\odot}$ (in agreement with [Hryniewicz et al. 2010](#)); the velocity shifts suggest the presence of strong outflows due to near- or super-Eddington accretion (i.e. with mechanical luminosity $> L_{\text{Edd}} \sim (6 - 12) \times 10^{47} \text{erg s}^{-1}$). It may represent the luminous quasar phase which [Yu & Tremaine \(2002\)](#) associate with rapid black hole growth.

If PG1407+265 were in a large galaxy cluster, the existence of such a wind would make it a good candidate to exemplify models such as that of [King \(2009\)](#) where it is proposed that the super-Eddington wind from an AGN with a mass in excess of $10^9 M_\odot$ is the source of cluster reheating. Contrariwise, evidence for a cool core cluster would suggest that quasar mode heating is unlikely to be widespread. This motivated the search, discussed below, for an associated cluster of galaxies.

Early quasar surveys relied on the strong emission lines of typical quasars for their discovery. Weak-line quasars, with CIV equivalent width less than 10\AA , are rare. One other relatively bright weak-lined object, PHL 1811 ([Leighly et al. 2007](#)) has been extensively studied, but it is notable for its *weak* X-ray emission. [Luo et al. \(2015\)](#) and [Ni et al. \(2018\)](#) identify further WLQs and investigated the prevalence of unusually weak X-ray emission in the group. [Luo et al. \(2015\)](#) also describe a class of consistently X-ray-weak so-called ‘PHL 1811’ analogs (see also [Shemmer et al. 2009](#), [Plotkin et al. 2010](#), [Wu et al. 2012](#)). They present evidence that the latter group (but not PHL 1811 itself) and about half of their WLQ sample are X-ray-weak due to obscuration by outflowing material that also shields the disk from the central object. If the shielding material does not block the line of sight, one observes an X-ray-normal WLQ; about half of the [Luo et al. \(2015\)](#) WLQ sample were X-ray normal WLQs. PG1407+265 is consistent with this scenario as one of the X-ray normal WLQs, because it is viewed mostly face-on and obscuration is less likely. The other X-ray-normal WLQs, such as the much less luminous 19th-magnitude SDSS J110938.50+373611.7 ([Plotkin et al. 2008](#), [Wu et al. 2012](#)) at $z=0.4$, are comparatively faint; PG1407+265 is the nearest exemplar of the class and is the only one whose X-ray count rate is enough for detailed study.

The model of PG1407+265 as largely face-on is supported by the multi-epoch radio study of [Blundell et al. \(2003\)](#). They presented evidence suggesting that the object is an intrinsically radio-quiet quasar amplified by a stunted pole-on relativistic radio jet. The jet’s two main radio knots are separated by a projected distance of 20 pc (2.5 mas), and there is no evidence for radio jet activity on kpc scales. The small physical scale of the jet suggests that the object may be related to GPS/CSS sources ([O’Dea & Saikia 2020](#)) and radio-quiet-to-loud transition objects ([Nyland et al. 2020](#), [Wołowska et al. 2021](#)).

3. OBSERVATIONS

3.1. *Reanalysis of the XMM observations*

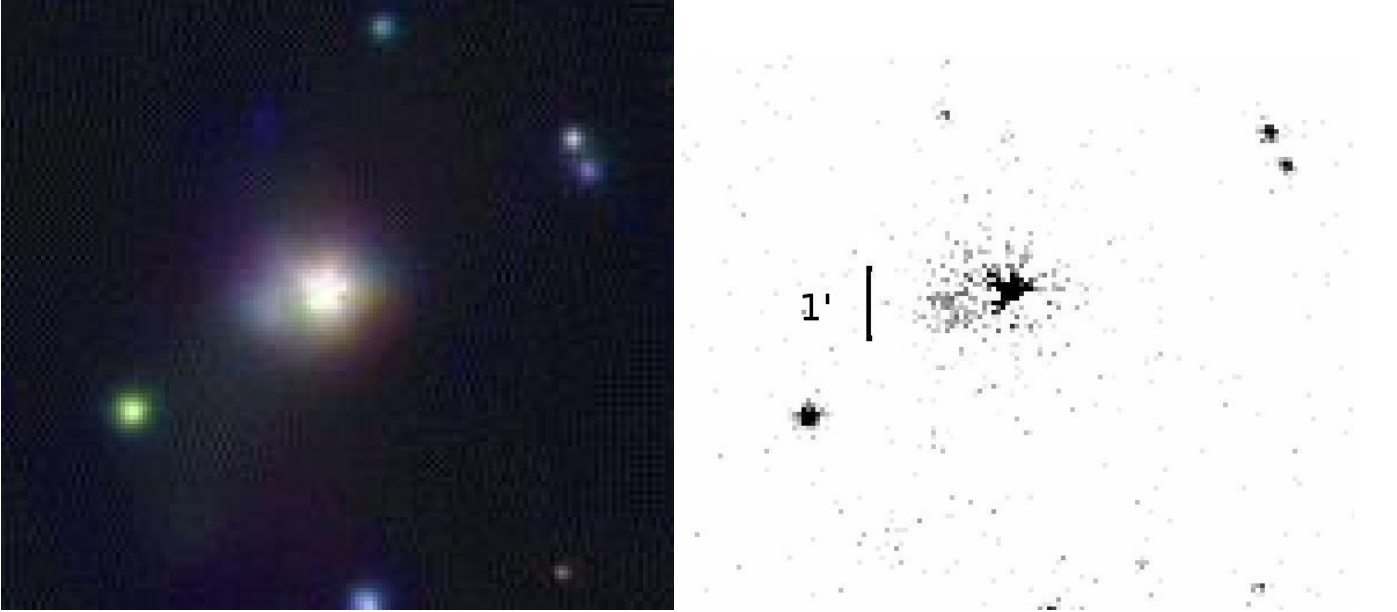


Figure 5. (a) XMM 41 ks MOS1 three-color image, showing extended emission on 1 arcmin (500 kpc) scales coincident with scale of optical cluster. (b) XMM 41 ks MOS1 image with partial PSF subtraction, showing extended emission. The scale bar length is 1 arcmin. North is at top in both images.

We reexamined the 2001 XMM observations of the quasar previously reported by Gallo (2006). The standard SAS archival data products were used (ESA:XMM-Newton SOC 2019). We used PSFs generated from HR1099 and from PKS0558-504 data and manually scaled to match the central regions of the PG1407+265 data; the results were similar in both cases. In the second XMM observation the quasar was significantly fainter than in the first one. In the XMM MOS1 and MOS2 data taken while PG1407+265 was in this lower state we detect faint, mildly asymmetric extended emission out to one arcminute radius (~ 500 kpc) after PSF subtraction (see Fig. 5). We interpret this emission as a luminous X-ray cluster.

The Sloan z -band image of PG1407+265 shows numerous faint galaxies within the XMM PSF and Blundell et al. (2003) detect radio emission from several, suggesting that a cluster can be identified with the extended emission. The low state X-ray luminosity of PG1407+265 measured by XMM is some $8 \times 10^{45} \text{ erg s}^{-1}$ which is comparable to the most luminous X-ray clusters (e.g. RXJ 1347.5-1145, Schindler et al. (1995)), so it is not unreasonable that cluster emission could contribute significantly to the total X-ray flux. From the XMM data we estimated that the cluster X-ray luminosity is at least a few $10^{44} \text{ erg s}^{-1}$ but with large and hard-to-quantify uncertainty, because the difficulty of removing the large XMM PSF makes a flux determination unreliable. We therefore carried out *Chandra* observations to investigate the cluster in more detail.

3.2. Chandra observations of the quasar

On 2017 Mar 14 we made a 41.5 ks observation of the PG1407+265 region using the *Chandra* ACIS (Advanced CCD Imaging Spectrometer, Garmire et al. (2003)) camera, ObsID 18265. The object was placed on chip 7 (S3) and a 1/2 subarray was used (i.e. reading out the central 512 columns of the 1024-pixel-wide chip). The resulting 512-pixel-wide strip gives enough area to ensure a good local background measurement while being narrow enough to reduce the pileup of the central AGN (*Chandra X-ray Center, Chandra Project Science MSFC and Chandra IPI Teams 2019*). The data were reduced using CIAO 4.12 and 4.13 (Fruscione et al. 2006, *Chandra X-ray Center 2020*).

The quasar was detected in a low state with 2077 net counts in the broad (0.5-7 keV) ACIS band. Using Sherpa (Freeman et al. 2001), we fit a power-law model over the 0.5-7 keV range to a PHA (instrumental energy channel) spectrum extracted in a 2-arcsecond radius circle and grouped to 15 counts per bin, using a chi-squared statistic and the ‘levmar’ fitting algorithm. A fixed Galactic absorption of $1.38 \times 10^{20} \text{ cm}^{-2}$ was assumed (McDowell et al. 1995). An energy-dependent aperture correction of less than 10 percent was applied to the effective area by the standard *specextract* script. The fit, shown in Fig. 6, gives a power-law photon spectral index of 2.26 ± 0.06 and the unabsorbed flux was found to be $F(0.5 - 10 \text{ keV}) = 5.26 \pm 0.48 \times 10^{-13} \text{ erg cm}^{-2} \text{ s}^{-1}$ (90 percent confidence interval using the `sample_energy_flux` routine in *Sherpa*). We checked that fitting instead using the simplex method and the Cash statistic is consistent with these results within the errors. There is no evidence for intrinsic absorption at the quasar redshift (adding such an absorber to the fit gives $N_H(\text{intrinsic}) < 10^{21} \text{ cm}^{-2}$). Restricting the fitting range to rest frame 2-10 keV gives a similar spectral slope of 2.14 ± 0.08 ; on the Risaliti et al. (2009) correlation of X-ray spectral slope with Eddington ratio this would correspond to $L/L_{\text{Edd}} \sim 0.4$, consistent with our suggestion that the object is near-Eddington and with the observation of similarly high spectral slopes for the ‘X-ray normal’ WLQs studied by Marlar et al. (2018).

The derived flux is a factor of 4 lower than in the previous faintest state in which the object has been seen (in 2001). The count rate is fairly stable during the observation, with a 12% drop from 0.050 to 0.044 counts s^{-1} for the last 10 ks of the exposure.

A probable iron line is detected with an observed energy of $3.56 \pm 0.05 \text{ keV}$ and an observed frame equivalent width of 0.14 keV (0.27 keV rest frame). If this is the Fe $K\alpha$ line with rest energy 6.4 keV, the corresponding redshift is 0.80 which would correspond to a blueshift of 27000 km s^{-1} relative to the inferred systemic velocity, a factor of two larger than the outflow velocities seen in the UV lines. Alternatively, if the feature shares the systemic velocity it would correspond to emission at $6.98 \pm 0.1 \text{ keV}$. The observed flux of the line is $7.3 \times 10^{-15} \text{ erg cm}^{-2} \text{ s}^{-1}$ and its FWHM is unconstrained. The line is not seen in the XMM spectra because of the higher continuum level during those observations. Refitting the XMM data indicates the line we observe in *Chandra* would have needed to be ~ 5 times brighter to be detectable.

3.3. The foreground cluster: optical observations

To the east of the quasar lies a $1'0 \times 1'5$ region of diffuse X-ray emission with a total of about 400 net counts. The peak of the diffuse X-ray emission is at 14:09:27.9 +26:18:13 (ICRS), close to (only about $5''$ south of) the $z = 0.68$

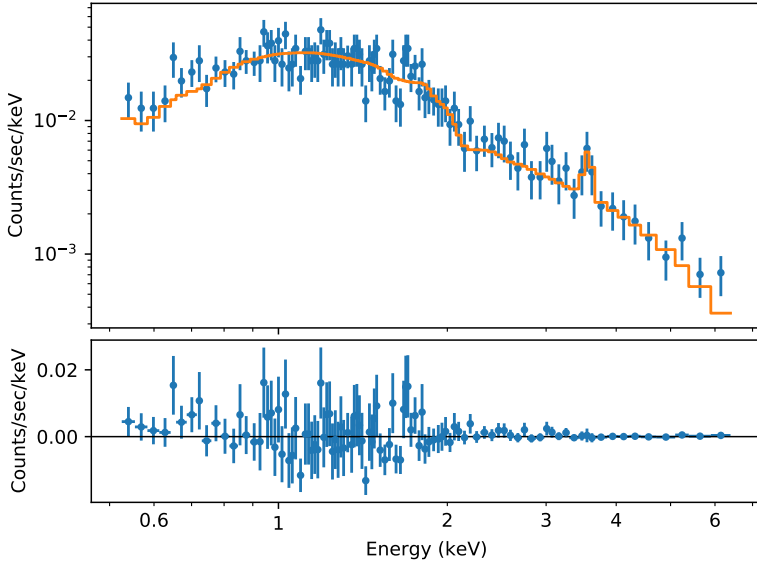


Figure 6. ACIS X-ray spectrum. Absorbed power law fit to the QSO spectrum, with an additional gaussian Fe line, using the Sherpa fitting package within CIAO. Upper panel: counts and fitted model; lower panel: residuals.

radio galaxy FIRST J140927.8+261818. We interpret the emission as due to hot gas in a cluster of galaxies associated with the radio galaxy.

By the Chandra naming convention, this cluster’s formal name is CXOU J140927.9+261813; however for ease of reading we will also refer to it in this paper as the East cluster, distinguishing it from a putative West cluster centered on and associated with PG1407+265 itself.

To understand the galaxy redshift distribution in the field and establish the redshift of the East cluster, we carried out optical observations in 2019 Apr with the BINOSPEC fiber spectrograph on the MMT. Prior to our investigation only the radio galaxy had a published spectroscopic redshift. There are about 50 further SDSS galaxies of similar optical magnitude in the field. SDSS estimates photometric redshifts for most of the remaining objects, but these have large uncertainties. A number of these photometric redshifts are within two sigma of the radio source redshift, hinting at possible cluster membership or large scale structure associated with the cluster. Numerous faint galaxies are visible on an image taken by the Hubble Space Telescope’s Advanced Camera for Surveys (ACS) (ACS-WFC1, F814W filter, sequence [JCWI06010](#), observation date 2016 May 4; [Lehner \(2015\)](#); Figure 8); these could also be cluster members.

For our followup spectroscopic observations BINOSPEC was configured with the 270 lines mm^{-1} grating ([Fabricant et al. 2019](#)). At $1.3 \text{ \AA pixel}^{-1}$ and a 1 arcsecond wide slitlet, nominal resolution is $R = 1340$ corresponding to about 250 km s^{-1} in the observed frame. Unfortunately as a result of bad weather we only observed 12 objects, of which four are possibly associated with the radio galaxy.

The BINOSPEC spectra were reduced using the standard BINOSPEC pipeline which extracts wavelength-calibrated spectra for each slit ([Kansky et al. 2019](#)). In almost all the objects, the 4000 \AA break and the Ca H and K lines allow an unambiguous redshift identification; we then estimated the redshift value by measuring H and K, and in most cases confirmed the value by also measuring the G band feature (4300 \AA), $\text{H}\beta$, $\text{H}\delta$, Mg I 5175 \AA , and Na D. We estimate the redshift accuracy is of order ± 0.001 . The three serendipitous *Chandra* sources, reported here for the first time and denoted X1 to X3 in Table 2, also have narrow OII 3727 and OIII 5007 emission lines.

Table 2 gives our internal source candidate identifier, the source name, the photometric redshift from SDSS, and our spectroscopic redshift measurement. The table also includes SDSS objects whose photometric redshifts are close to 0.7 and thus are possible cluster members (C05 is the radio source suspected to be the cluster center). A finding chart for the sources overlaid on the HST ACS image is presented in Figure 8. The existence of several objects with z near 0.68 within the X-ray contours, together with the possible $z = 0.68$ Fe line in the cluster X-ray spectrum and the

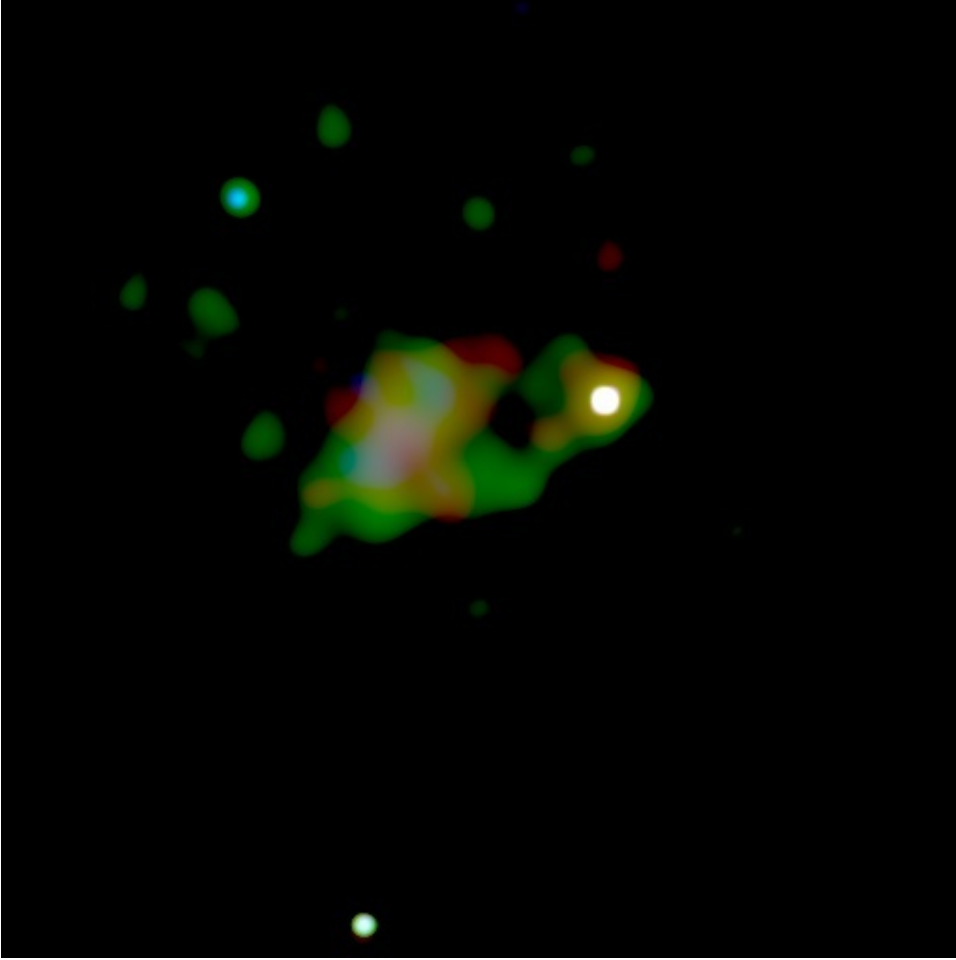


Figure 7. Adaptively smoothed X-ray color image of the *Chandra* data showing the arcminute-scale diffuse emission. The standard CSC energy bands are used: Red: 0.3-1.2 keV; Green: 1.2-2.0 keV; Blue: 2.0-7.0 keV. North is at top.

known $z = 0.68$ UV absorption feature in the quasar, lead us to propose that the redshift of the East cluster CXOU J140927.9+261813 is indeed $z = 0.68$.

3.4. *Chandra observations of the East cluster: spectrum and radial profile*

We filtered the X-ray event list into three energy bands (the standard Chandra Source Catalog bands of 0.3-1.2 keV, 1.2-2.0 keV, and 2.0-7.0 keV, [Evans et al. 2010](#)) to look for spatial variations of the X-ray spectrum. The energy boundaries were chosen to give reasonable signal-to-noise in each band. We then adaptively smoothed each of the three bands separately with the CIAO *csmooth* tool. The resulting three-band background-subtracted X-ray color image of the field is shown in Fig. 7; the apparent spectral variations are not statistically significant.

We also extracted a spectrum from the event file in a polygonal region surrounding the East cluster diffuse emission. The spectrum has 345 net counts within this extraction region in the 0.5-7 keV band. A 5-arcsecond-radius region around the quasar was excluded; no other point sources were detected within the diffuse emission region. We fit an APEC (Astrophysical Plasma Emission Code, [Smith et al. 2001](#)) model with solar abundances, a redshift of 0.68, and the fixed Galactic absorption (Fig. 9). Due to the low number of counts, we performed a simplex fit using the Cash statistic; the background was fit separately and modelled as a power law with an additional line at 1.75 keV.

The source's temperature is weakly constrained at $2.9^{+1.6}_{-0.9}$ keV, and allowing the abundance to vary does not change the overall fit significantly. However, an emission feature is visible at 4.0 keV which is well fit by the redshifted 6.7 keV iron line produced by the model, as long as the metallicity is around solar or greater. We note this metallicity is larger than the typical metallicity for non-cool-core clusters of 0.2 reported by [Allen & Fabian \(1998\)](#). The line suggests that the cluster may indeed be at the redshift of the radio galaxy (see further, below). Adding two other

ID	Name	z_p	z
Chandra sources			
X1	CXOU J140931.0+261913		0.599
X2	CXOU J140919.5+261820		0.460
X3	CXOU J140921.0+261816		0.327
Candidate cluster members			
C02	SDSS J140929.25+261808.5	0.63	0.671
C03	SDSS J140927.93+261807.3	0.57	-
C05	SDSS J140927.84+261818.7	0.45	0.68 (SDSS)
C08	SDSS J140927.33+261837.5	0.71	-
C09	SDSS J140926.56+261833.2	0.61	-
C10	SDSS J140925.45+261831.1	0.62	0.680
C11	SDSS J140924.78+261824.8	0.78	0.681
C19	SDSS J140925.06+261917.6	0.53	-
C20	SDSS J140924.73+261917.4	0.77	-
C23	SDSS J140924.61+261844.5	0.62	-
C24	SDSS J140923.92+2618378	0.56	-
C38	SDSS J140920.22+261849.7	0.70	-
C47	SDSS J140921.86+261736.9	0.59	-
C49	SDSS J140919.99+261727.0	0.57	0.658
C51	SDSS J140919.94+261647.6	0.56	-
C56	SDSS J140923.73+261715.7	0.56	-
C58	SDSS J140925.31+261717.2	0.72	-
C67	SDSS J140926.93+261755.8	0.71	-
C70	SDSS J140929.86+261733.9	0.66	-
C75	SDSS J140931.05+261913.9	0.74	-
Other sources in field			
C04	SDSS J140927.43+261807.2		0.375
C06	SDSS J140927.86+261822.2	0.47	0.435
C15	SDSS J140928.82+261931.6	0.29	0.328
C73	SDSS J140930.85+261755.6	0.40	0.374
H1	Anon 140923.9+261812		0.114

Table 2. Estimated redshifts of sources in the PG1407+265 field. The ID is an internal source identifier; z_p is the SDSS photometric redshift and z is the spectroscopic redshift (from our MMT observations except where noted). We identify object X1 with optical source SDSS J140931.05+261913.9.

lines at observed energies of 2.77 and 5.49 keV improves the fit somewhat. At the radio galaxy redshift these would correspond to 4.65 keV and 9.22 keV respectively; we are unable to propose interpretation of these features. Using the MEKAL (Mewe-Kaastra-Leidahl, [Mewe et al. 1985](#)) model instead of APEC gives a very similar fit.

The unabsorbed flux of the cluster (i.e., the flux corrected for Galactic foreground absorption) is $F(0.5 - 2\text{keV}) = (3.6 \pm 0.2) \times 10^{-14} \text{erg cm}^{-2} \text{s}^{-1}$ and $F(2 - 10\text{keV}) = (6.5 \pm 1.3) \times 10^{-14} \text{erg cm}^{-2} \text{s}^{-1}$ (90 percent confidence intervals, using the *Sherpa sample.energy.flux* command).

If the cluster is at the radio galaxy distance, $L(0.1 - 2.4\text{keV}) = (6.8 \pm 0.6) \times 10^{43} \text{erg s}^{-1}$. Estimates of the flux and luminosity of the quasar and cluster are given in Table 3.

Using the temperature-mass relationship derived by [Finoguenov et al. \(2001\)](#) for objects with temperatures above 3 keV, we infer a cluster mass $\log(M/M_\odot) = 14.3^{+0.4}_{-0.5}$ within the conventional r_{500} radius at which the density drops below 500 times the cosmological critical density at $z = 0.68$.

We also extracted a radial X-ray surface brightness profile for the East cluster. An exposure-corrected image was created in the 0.5–7 keV band using the CIAO *fluximage* script. To prevent contamination of the profile by the bright quasar itself, a circular region of $10''$ radius centered on PG1407+265 was first replaced by photons sampled

	Energy band (keV)	Quasar	East Cluster
Assumed redshift z		0.96	0.68
Unabsorbed flux (10^{-13} erg cm $^{-2}$ s $^{-1}$)	0.5-2 (obs)	2.88 ± 0.18	0.36 ± 0.02
Unabsorbed flux (10^{-13} erg cm $^{-2}$ s $^{-1}$)	2-10 (obs)	2.38 ± 0.37	0.65 ± 0.13
Luminosity (10^{44} erg s $^{-1}$)	0.1-2.4 (rest)	48.4 ± 2.8	0.68 ± 0.06
Luminosity (10^{44} erg s $^{-1}$)	2-10 (rest)	14.0 ± 3.8	1.4 ± 0.2
Luminosity (10^{44} erg s $^{-1}$)	0.1-10 (rest)	60.6 ± 4.3	2.0 ± 0.2

Table 3. Fitted fluxes and luminosities for the quasar and cluster in soft and hard bands. Values and uncertainties are medians and 90% confidence intervals derived from the *Sherpa* `sample_energy_flux` routine. Luminosities for the quasar at rest frame energies below 1 keV are provided for comparison with other sources but are an extrapolation of the fit and therefore not reliable. Luminosities for the cluster have uncertainties of 8%, with roughly equal contribution from the Poisson error (low number of counts) and the fitting uncertainty in the temperature.

from the same radial distance from the cluster center using the CIAO tool *dmfilth*. All the regions were visually inspected to verify that they were not contaminated by bright sources, and that they did not extend outside the bounds of the exposed areas of the ACIS detectors. The exposure-corrected cluster X-ray surface brightness in the 0.5–7 keV band was then measured in concentric 5''-wide annuli centered on the peak of the diffuse emission using the CIAO tool *dmextract*. A background region 1'5 away was used to subtract a constant component. The resulting background-subtracted radial surface brightness profile for CXOU J140927.9+261813 is shown in Fig. 10.

The X-ray surface brightness profile for CXOU J140927.9+261813 was fit with a beta model using *Sherpa*. Formally the profile is poorly constrained by the global fit (Fig 10, right panel), but examination of residuals for an ensemble of fits suggests that a core radius of 15 to 35 arcsec and a beta value of 0.6 to 1.0 provide a reasonable representation of the data. A representative fit with core radius 20 arcsec and $\beta = 0.70$ is overplotted on the measurements in Fig. 10. Using an isothermal hydrostatic equilibrium model, the mass within 500 kpc derived from this fit is found to be $\log(M(500\text{kpc})/M_{\odot}) = 14.2 \pm 0.4$. This is consistent with the simple mass-temperature relation used earlier although we note the 500 kpc radius used is different from that relation's r_{500} radius, whose value is poorly constrained in our data. The amplitude of the fitted profile is, however, well-constrained: $S_0 = 1.8 \pm 0.2 \times 10^{-8}$ photons cm $^{-2}$ s $^{-1}$ arcsec $^{-2}$ and there is no evidence of a cuspy central peak, so we infer that the cluster is a non-cool-core one.

3.5. Cluster Lensing

McDowell et al. (1995) raised the possibility that the unusual nature of PG1407+265 might in part be due to lensing by a foreground object. The discovery of exactly such a foreground object prompted us to re-examine this possibility in light of the newly available *Chandra* observations.

Our derived East cluster mass of $\log(M/M_{\odot}) = 14.3^{+0.4}_{-0.5}$ corresponds to an Einstein radius of 0.1 to 0.3 arcmin, compared to the cluster-center-to-quasar distance of about 1 arcmin. This argues against significant lensing of the quasar PG1407+265 by the cluster CXOU J140927.9+261813, but deeper observations will be needed to conclude this with confidence.

3.6. The West cluster: radial profile analysis

The diffuse emission near the quasar could be foreground emission from the East cluster, in which case this cluster has a disturbed morphology and is far from virialized - possibly, even, two clusters merging. We note that the dark ‘bay’ between the main East cluster and the emission near the quasar is significant (in a 7 arcsecond circle, total broad band counts are only 24 compared to 40 in adjoining areas of equal size).

An alternative possibility is that the emission near the quasar is a second cluster - we will call it the West cluster - centered on the quasar and at its redshift. We do not have enough counts in the western emission to detect the putative Fe line in that region. We therefore searched for evidence of a peak in the extended emission around the quasar point source, but the current data do not give us a definitive answer: there is no clear evidence of extent in the quasar image at the few arcsecond scale. In Fig 11 we show the radial profile of the 0.5-7 keV count surface brightness distribution centered on the quasar and compare it with a point spread function made using the ChaRT (Carter et al. 2003) and MARX (Davis et al. 2012) PSF simulation tools. The PSF shown is the average of five realizations and is normalized by matching the data at a radius of 0.5 arcseconds. It can be seen that the PSF is slightly narrower

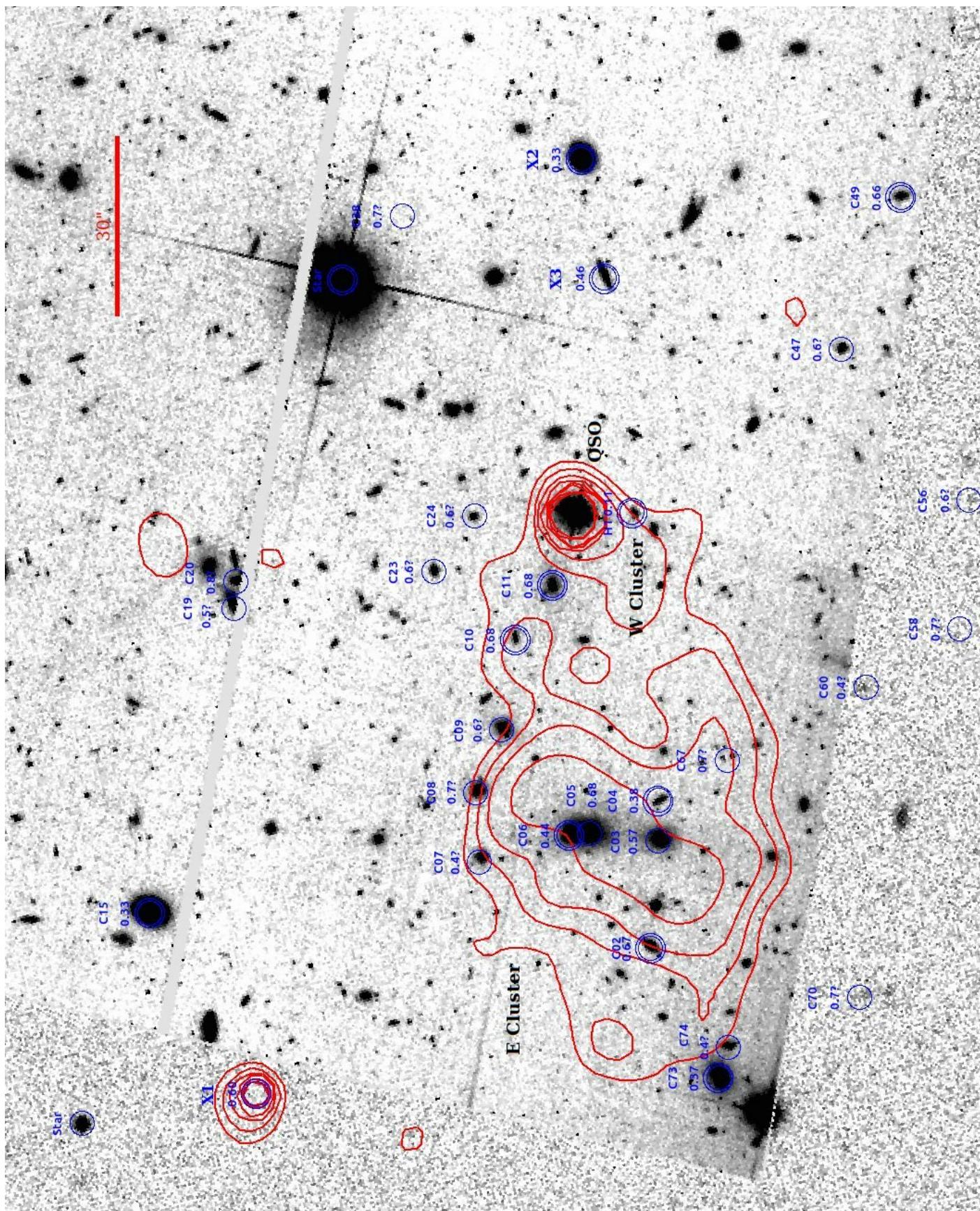


Figure 8. HST ACS image (Lehner 2015) overlaid on SDSS g-band image, showing X-ray contours (red) with position of quasar and of the East cluster, and indicating galaxies with spectroscopic (blue double circles) and photometric (blue single circles) redshifts potentially associated with the East cluster. Identifiers correspond to those in Table 2. Scale bar at top right has a length of 30 arcseconds.

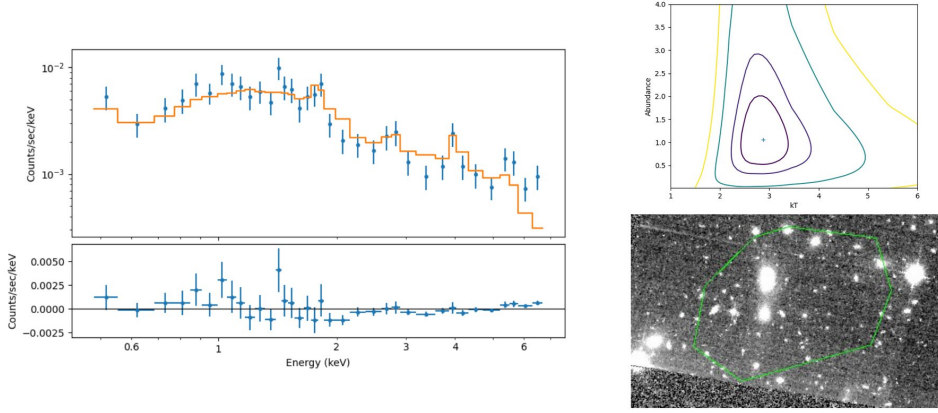


Figure 9. Left panel: APEC fit to the nebular (East cluster) spectrum assuming $z = 0.68$, showing a redshifted iron line and two other possible features. The best fit temperature is poorly constrained, $kT = 2.9^{+1.6}_{-0.9}$ keV. Right upper panel: 0.5, 1, 2 and 3 sigma reduced χ^2 contours (relative to best fit) versus temperature and abundance for APEC model spectral fit. Right lower panel: ACIS image of region with extraction region overlaid (green polygon).

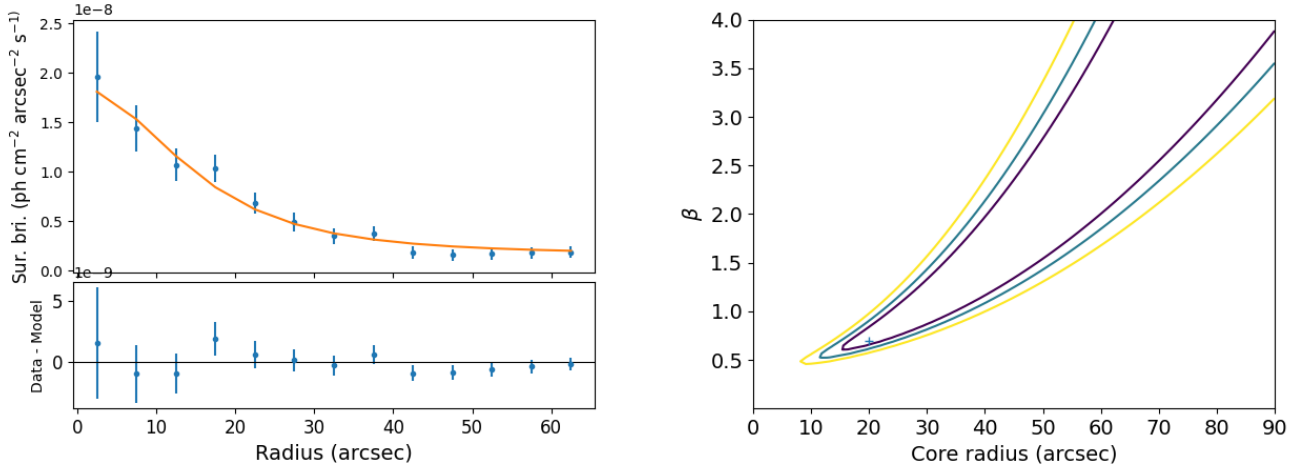


Figure 10. Left: Cluster radial profile and fit. The x axis gives the radius from the X-ray peak in arcseconds; the y axis is the 0.5–7.0 keV surface brightness in $10^{-8}\text{ph cm}^{-2} \text{arcsec}^{-2} \text{s}^{-1}$. Residuals are shown in the lower left panel. Right: 1, 2 and 3 sigma contours of reduced χ^2 for the cluster radial profile fit, as a function of core radius in arcseconds (x axis) and beta (y axis). The parameters are weakly constrained.

than the data, and there is some suggestion of excess flux near 1 to 2 arcseconds, but we conclude that there is no definite evidence of extent except beyond 10 arcseconds. Nevertheless, the statistical errors would allow the presence of a diffuse source with a luminosity of order 10^{44}erg s^{-1} .

A deeper exposure will be needed to decide whether the western emission is part of the East cluster or is from a West cluster associated with PG1407+265 itself.

4. CONCLUSION

A quarter-century after the study of McDowell et al. (1995) the PG1407+265 system remains rather enigmatic but some aspects of it have come into focus. The face-on but stunted radio jet may indicate that the quasar is a failed blazar (Blundell et al. 2003, McDowell et al. 1995) with a broader rapid outflow explaining the extreme line shifts. These shifts seen at UV and, possibly, X-ray wavelengths could even be due to interaction with the weak but relativistic radio

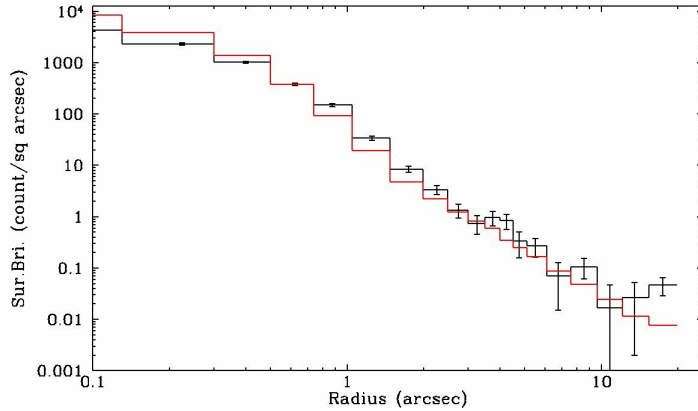


Figure 11. Broad-band (0.5-7 keV) X-ray radial profile centered on the quasar. Black line: log of extracted surface brightness versus log radial distance from center. Red line: Chart/MARX PSF radial profile with normalization matched at 1 pixel (0.5 arcseconds). A possible excess near 1-2 arcseconds is within the uncertainties of the PSF normalization.

jet; future work is needed to explore this possibility. The almost-line-of-sight galaxy cluster CXOU J140927.9+261813 complicates the picture but the observations suggest that we cannot explain away the low equivalent width lines as being due to lensing. The existence of X-ray emission from a second cluster at the redshift of the quasar is ambiguous. The previous absence of these clusters from cluster catalogs due to the glare of the quasar emphasizes the importance of high spatial resolution X-ray imaging of the kind provided by *Chandra* and proposed for *Lynx*.

5. ACKNOWLEDGEMENTS

This work was supported by Chandra grant GO6-17117X and by the NASA Chandra X-ray Center, which is operated by the Smithsonian Astrophysical Observatory for and on behalf of the National Aeronautics Space Administration under contract NAS8-03060. We thank MMTO/TDC staff for making the MMT observations and processing the data through the standard pipeline. We also thank R. Saxton for advice on the XMM PSF and D. Burke and B. Wilkes for helpful comments. We acknowledge the use of the software packages SAS (ESA:XMM-Newton SOC 2019), CIAO (Fruscione et al. 2006, Chandra X-ray Center 2020), Sherpa (Freeman et al. 2001) and DS9 (Joye & Mandel 2003), as well as Ned Wright’s cosmology calculator (Wright 2006). This research has made use of the NASA/IPAC Infrared Science Archive, which is operated by the Jet Propulsion Laboratory, California Institute of Technology, under contract with the National Aeronautics and Space Administration; the SIMBAD database, operated at CDS, Strasbourg, France, and NASA’s Astrophysics Data System Bibliographic Services. This publication makes use of data products from the Wide-field Infrared Survey Explorer, which is a joint project of the University of California, Los Angeles, and the Jet Propulsion Laboratory/California Institute of Technology, and NEOWISE, which is a project of the Jet Propulsion Laboratory/California Institute of Technology. WISE and NEOWISE are funded by the National Aeronautics and Space Administration. The Catalina photometry is courtesy of the CSS survey, funded by the National Aeronautics and Space Administration under Grant No. NNG05GF22G issued through the Science Mission Directorate Near-Earth Objects Observations Program.

We thank the anonymous referee for their helpful comments on the initial version of this paper.

This is the Accepted Manuscript version of an article accepted for publication in the *Astrophysical Journal*. IOP Publishing Ltd is not responsible for any errors or omissions in this version of the manuscript or any version derived from it. The Version of Record will be available online at <https://iopscience.iop.org/journal/0004-637X>

REFERENCES

- Allen, S. W., & Fabian, A. C. 1998, *MNRAS*, 297, L63, doi: [10.1046/j.1365-8711.1998.01738.x](https://doi.org/10.1046/j.1365-8711.1998.01738.x)
- Barvainis, R., Lonsdale, C., & Antonucci, R. 1996, *AJ*, 111, 1431, doi: [10.1086/117888](https://doi.org/10.1086/117888)
- Blundell, K. M., Beasley, A. J., & Bicknell, G. V. 2003, *ApJL*, 591, L103, doi: [10.1086/377295](https://doi.org/10.1086/377295)
- Carter, C., Karovska, M., Jerius, D., Glotfelty, K., & Beikman, S. 2003, in *Astronomical Society of the Pacific Conference Series*, Vol. 295, *Astronomical Data Analysis Software and Systems XII*, ed. H. E. Payne, R. I. Jedrzejewski, & R. N. Hook, 477
- Chandra X-ray Center. 2020, CIAO 4.13. <https://cxc.cfa.harvard.edu/ciao/index.html>
- Chandra X-ray Center, Chandra Project Science MSFC and Chandra IPI Teams. 2019, Chandra Proposers' Observatory Guide, Version 22.0, Tech. rep., CXC. <https://cxc.harvard.edu/proposer/POG/html/index.html>
- Cutri, R. M., Wright, E. L., Conrow, T., et al. 2013, Explanatory Supplement to the AllWISE Data Release Products, Explanatory Supplement to the AllWISE Data Release Products
- Davis, J. E., Bautz, M. W., Dewey, D., et al. 2012, in *Society of Photo-Optical Instrumentation Engineers (SPIE) Conference Series*, Vol. 8443, *Space Telescopes and Instrumentation 2012: Ultraviolet to Gamma Ray*, ed. T. Takahashi, S. S. Murray, & J.-W. A. den Herder, 84431A, doi: [10.1117/12.926937](https://doi.org/10.1117/12.926937)
- Drake, A. J., Djorgovski, S. G., Mahabal, A., et al. 2009, *ApJ*, 696, 870, doi: [10.1088/0004-637X/696/1/870](https://doi.org/10.1088/0004-637X/696/1/870)
- Ellingson, E., Yee, H. K. C., & Green, R. F. 1991, *ApJ*, 371, 49, doi: [10.1086/169869](https://doi.org/10.1086/169869)
- Elvis, M., Wilkes, B. J., McDowell, J. C., et al. 1994, *ApJS*, 95, 1, doi: [10.1086/192093](https://doi.org/10.1086/192093)
- ESA:XMM-Newton SOC. 2019, Users Guide to the XMM-Newton Science Analysis System
- Evans, I. N., Primi, F. A., Glotfelty, K. J., et al. 2010, *ApJS*, 189, 37, doi: [10.1088/0067-0049/189/1/37](https://doi.org/10.1088/0067-0049/189/1/37)
- Fabricant, D., Fata, R., Epps, H., et al. 2019, *PASP*, 131, 075004, doi: [10.1088/1538-3873/ab1d78](https://doi.org/10.1088/1538-3873/ab1d78)
- Finoguenov, A., Reiprich, T. H., & Böhringer, H. 2001, *A&A*, 368, 749, doi: [10.1051/0004-6361:20010080](https://doi.org/10.1051/0004-6361:20010080)
- Freeman, P., Doe, S., & Siemiginowska, A. 2001, in *Society of Photo-Optical Instrumentation Engineers (SPIE) Conference Series*, Vol. 4477, *Astronomical Data Analysis*, ed. J.-L. Starck & F. D. Murtagh, 76–87, doi: [10.1117/12.447161](https://doi.org/10.1117/12.447161)
- Frusciione, A., McDowell, J. C., Allen, G. E., et al. 2006, in *Society of Photo-Optical Instrumentation Engineers (SPIE) Conference Series*, Vol. 6270, *Society of Photo-Optical Instrumentation Engineers (SPIE) Conference Series*, ed. D. R. Silva & R. E. Doxsey, 62701V, doi: [10.1117/12.671760](https://doi.org/10.1117/12.671760)
- Gallo, L. C. 2006, *MNRAS*, 365, 960, doi: [10.1111/j.1365-2966.2005.09780.x](https://doi.org/10.1111/j.1365-2966.2005.09780.x)
- Garmire, G. P., Bautz, M. W., Ford, P. G., Nousek, J. A., & Jr., G. R. R. 2003, in *X-Ray and Gamma-Ray Telescopes and Instruments for Astronomy*, ed. J. E. Truemper & H. D. Tananbaum, Vol. 4851, *International Society for Optics and Photonics (SPIE)*, 28 – 44, doi: [10.1117/12.461599](https://doi.org/10.1117/12.461599)
- Gibson, R. R., Brandt, W. N., & Schneider, D. P. 2008, *ApJ*, 685, 773, doi: [10.1086/590403](https://doi.org/10.1086/590403)
- Hryniewicz, K., Czerny, B., Nikolajuk, M., & Kuraszkiewicz, J. 2010, *MNRAS*, 404, 2028, doi: [10.1111/j.1365-2966.2010.16418.x](https://doi.org/10.1111/j.1365-2966.2010.16418.x)
- Joye, W. A., & Mandel, E. 2003, in *Astronomical Society of the Pacific Conference Series*, Vol. 295, *Astronomical Data Analysis Software and Systems XII*, ed. H. E. Payne, R. I. Jedrzejewski, & R. N. Hook, 489
- Kansky, J., Chilingarian, I., Fabricant, D., et al. 2019, Binospec: Data reduction pipeline for the Binospec imaging spectrograph. <http://ascl.net/1905.004>
- King, A. 2009, *ApJL*, 695, L107, doi: [10.1088/0004-637X/695/1/L107](https://doi.org/10.1088/0004-637X/695/1/L107)
- Lehner, N. 2015, HST Proposal 14269; Just the BASICS: Linking Gas Flows in the Circumgalactic Medium to Galaxies. https://archive.stsci.edu/proposal_search.php?id=14269&mission=hst
- Lehner, N., Wotta, C. B., Howk, J. C., et al. 2018, *ApJ*, 866, 33, doi: [10.3847/1538-4357/aadd03](https://doi.org/10.3847/1538-4357/aadd03)
- Leighly, K. M., Halpern, J. P., Jenkins, E. B., et al. 2007, *ApJ*, 663, 103, doi: [10.1086/518017](https://doi.org/10.1086/518017)
- Luo, B., Brandt, W. N., Hall, P. B., et al. 2015, *ApJ*, 805, 122, doi: [10.1088/0004-637X/805/2/122](https://doi.org/10.1088/0004-637X/805/2/122)
- Marculewicz, M., & Nikolajuk, M. 2020, *ApJ*, 897, 117, doi: [10.3847/1538-4357/ab9597](https://doi.org/10.3847/1538-4357/ab9597)
- Marlar, A., Shemmer, O., Anderson, S. F., et al. 2018, *ApJ*, 865, 92, doi: [10.3847/1538-4357/aad812](https://doi.org/10.3847/1538-4357/aad812)
- Massaro, E., Giommi, P., Leto, C., et al. 2009, *A&A*, 495, 691, doi: [10.1051/0004-6361:200810161](https://doi.org/10.1051/0004-6361:200810161)
- Massaro, F., D'Abrusco, R., Ajello, M., Grindlay, J. E., & Smith, H. A. 2011, *ApJL*, 740, L48, doi: [10.1088/2041-8205/740/2/L48](https://doi.org/10.1088/2041-8205/740/2/L48)
- McConnell, N. J., Ma, C.-P., Gebhardt, K., et al. 2011, *Nature*, 480, 215, doi: [10.1038/nature10636](https://doi.org/10.1038/nature10636)

- McConnell, N. J., Ma, C.-P., Murphy, J. D., et al. 2012, *ApJ*, 756, 179, doi: [10.1088/0004-637X/756/2/179](https://doi.org/10.1088/0004-637X/756/2/179)
- McDowell, J. C., Canizares, C., Elvis, M., et al. 1995, *ApJ*, 450, 585, doi: [10.1086/176168](https://doi.org/10.1086/176168)
- Mewe, R., Gronenschild, E. H. B. M., & van den Oord, G. H. J. 1985, *A&AS*, 62, 197
- Ni, Q., Brandt, W. N., Luo, B., et al. 2018, *MNRAS*, 480, 5184, doi: [10.1093/mnras/sty1989](https://doi.org/10.1093/mnras/sty1989)
- Nyland, K., Dong, D. Z., Patil, P., et al. 2020, *ApJ*, 905, 74, doi: [10.3847/1538-4357/abc341](https://doi.org/10.3847/1538-4357/abc341)
- O’Dea, C. P., & Saikia, D. J. 2020, arXiv e-prints, arXiv:2009.02750. <https://arxiv.org/abs/2009.02750>
- Planck Collaboration, Aghanim, N., Akrami, Y., et al. 2020, *A&A*, 641, A6, doi: [10.1051/0004-6361/201833910](https://doi.org/10.1051/0004-6361/201833910)
- Plotkin, R. M., Anderson, S. F., Brandt, W. N., et al. 2010, *ApJ*, 721, 562, doi: [10.1088/0004-637X/721/1/562](https://doi.org/10.1088/0004-637X/721/1/562)
- Plotkin, R. M., Anderson, S. F., Hall, P. B., et al. 2008, *AJ*, 135, 2453, doi: [10.1088/0004-6256/135/6/2453](https://doi.org/10.1088/0004-6256/135/6/2453)
- Reeves, J. N., & Turner, M. J. L. 2000, *MNRAS*, 316, 234, doi: [10.1046/j.1365-8711.2000.03510.x](https://doi.org/10.1046/j.1365-8711.2000.03510.x)
- Risaliti, G., Young, M., & Elvis, M. 2009, *ApJL*, 700, L6, doi: [10.1088/0004-637X/700/1/L6](https://doi.org/10.1088/0004-637X/700/1/L6)
- Russell, H. R., Fabian, A. C., Sanders, J. S., et al. 2010, *MNRAS*, 402, 1561, doi: [10.1111/j.1365-2966.2009.16027.x](https://doi.org/10.1111/j.1365-2966.2009.16027.x)
- Russell, H. R., Fabian, A. C., Taylor, G. B., et al. 2012, *MNRAS*, 422, 590, doi: [10.1111/j.1365-2966.2012.20637.x](https://doi.org/10.1111/j.1365-2966.2012.20637.x)
- Schindler, S., Guzzo, L., Ebeling, H., et al. 1995, *A&A*, 299, L9. <https://arxiv.org/abs/astro-ph/9505097>
- Schmidt, M., & Green, R. F. 1983, *ApJ*, 269, 352, doi: [10.1086/161048](https://doi.org/10.1086/161048)
- Serjeant, S., & Hatziminaoglou, E. 2009, *MNRAS*, 397, 265, doi: [10.1111/j.1365-2966.2009.14431.x](https://doi.org/10.1111/j.1365-2966.2009.14431.x)
- Shemmer, O., Brandt, W. N., Anderson, S. F., et al. 2009, *ApJ*, 696, 580, doi: [10.1088/0004-637X/696/1/580](https://doi.org/10.1088/0004-637X/696/1/580)
- Shen, Y., & Liu, X. 2012, *ApJ*, 753, 125, doi: [10.1088/0004-637X/753/2/125](https://doi.org/10.1088/0004-637X/753/2/125)
- Siemiginowska, A., Burke, D. J., Aldcroft, T. L., et al. 2010, *ApJ*, 722, 102, doi: [10.1088/0004-637X/722/1/102](https://doi.org/10.1088/0004-637X/722/1/102)
- Siemiginowska, A., Cheung, C. C., LaMassa, S., et al. 2005, *ApJ*, 632, 110, doi: [10.1086/432871](https://doi.org/10.1086/432871)
- Smith, R. K., Brickhouse, N. S., Liedahl, D. A., & Raymond, J. C. 2001, *ApJL*, 556, L91, doi: [10.1086/322992](https://doi.org/10.1086/322992)
- Somboonpanyakul, T., McDonald, M., Gaspari, M., Stalder, B., & Stark, A. A. 2021, arXiv e-prints, arXiv:2101.01730. <https://arxiv.org/abs/2101.01730>
- Tadhunter, C. 2008, *Mem. Soc. Astron. Italiana*, 79, 1205
- Tananbaum, H., Avni, Y., Branduardi, G., et al. 1979, *ApJL*, 234, L9, doi: [10.1086/183100](https://doi.org/10.1086/183100)
- Vestergaard, M., & Osmer, P. S. 2009, *ApJ*, 699, 800, doi: [10.1088/0004-637X/699/1/800](https://doi.org/10.1088/0004-637X/699/1/800)
- Williams, O. R., Turner, M. J. L., Stewart, G. C., et al. 1992, *ApJ*, 389, 157, doi: [10.1086/171194](https://doi.org/10.1086/171194)
- Wołowska, A., Kunert-Bajraszewska, M., Mooley, K. P., et al. 2021, arXiv e-prints, arXiv:2103.08422. <https://arxiv.org/abs/2103.08422>
- Wright, E. L. 2006, *PASP*, 118, 1711, doi: [10.1086/510102](https://doi.org/10.1086/510102)
- Wu, J., Brandt, W. N., Anderson, S. F., et al. 2012, *ApJ*, 747, 10, doi: [10.1088/0004-637X/747/1/10](https://doi.org/10.1088/0004-637X/747/1/10)
- Yu, Q., & Tremaine, S. 2002, *MNRAS*, 335, 965, doi: [10.1046/j.1365-8711.2002.05532.x](https://doi.org/10.1046/j.1365-8711.2002.05532.x)